Received: 28 February 2018 | Revised: 18 August 2018 | Accepted: 23 August 2018

DOI: 10.1111/ffe.12927

ORIGINAL CONTRIBUTION

WILEY

A computationally efficient cohesive zone model for fatigue

Sarmed Salih[2] | Keith Davey[1] | Zhenmin Zou[1]

[1]School of Mechanical, Aerospace and Civil Engineering, The University of Manchester, Manchester, UK

[2]College of Engineering, The University of Babylon, Babel, Iraq

Correspondence
Sarmed Salih, College of Engineering, The University of Babylon, Babel, Iraq
Email: eng.sarmed.salih@uobabylon.edu.iq

Funding information
The higher committee for education development in Iraq

Abstract

A cohesive zone model has been developed for the simulation of both high and low cycle fatigue crack growth. The developed model provides an alternative approach that reflects the computational efficiency of the well-established *envelop-load damage model* yet can deliver the accuracy of the equally well-established *loading-unloading hysteresis damage model*.

A feature included in the new cohesive zone model is a damage mechanism that accumulates as a result of cyclic plastic separation and material deterioration to capture a finite fatigue life. The accumulation of damage is reflected in the loading-unloading hysteresis curve, but additionally, the model incorporates a fast-track feature. This is achieved by "freezing in" a particular damage state for one loading cycle over a predefined number of cycles.

The new model is used to simulate mode I fatigue crack growth in austenitic stainless steel 304 at significant reduction in the computational cost.

KEYWORDS

cohesive model, fatigue crack growth modelling, UMAT subroutine

1 | INTRODUCTION

Engineering structures such as bridges, power plants, airplanes, trains, cars, and others have played an important role in human life since the beginning of the industrial revolution. However, these structures can suffer from mechanical failures caused by crack propagation leading potentially to catastrophic events, loss of human life, and significant financial cost. Fatigue phenomena have been the subject of research for more than 150 years. However, complete solutions for this issue have not yet been discovered.[1] Great effort has been made to understand and evaluate the crack growth behaviour under cyclic loading. However, fatigue remains an area of active research with the development of new materials and physical models. All current models used in the description of fatigue behaviour suffer from limitations, and none are able to capture the extensive experimental evidence available in the literature.

It is apparent from the academic literature that the cohesive zone model (CZM) is presently considered to be an attractive approach when combined with the finite element method to simulate fracture and fatigue problems. Nevertheless, an optimum CZM able to simulate

Nomenclature: a^{cz}, Cohesive zone length; D^c, Cyclic damage; D^s, Static damage; E, Elastic modulus; K^{coh}, Cohesive stiffness; G^c, Total dissipated energy per unit area; G^p, Dissipated plastic energy in the cohesive zone per unit area; N, Number of cycles; N^f, Number of cycles to fail the cohesive element; ΔN, Number of cycles in the load envelope; N^u, Number of required damage updates; I^o, Critical cohesive energy; δ^c, Critical separation; δ_1, Shape parameter for the linear and trapezoidal model respectively; δ_2, Second shape parameter of the trapezoidal model; δ^p, Plastic separation; δ^{cyc}, Cyclic separation; $\delta^{cyc^{max}}$, Maximum separation reached at the loading cycle; δ, Separation in the CE; δ^{max}, The separation at the onset of unloading; σ^c, Critical cohesive stress; σ, Cohesive stress; σ^Y, Yield stress; σ^{max}, The stress at the onset of unloading; ϑ, Poisson ratio

Abbreviation: CE, Cohesive element; CZ, Cohesive zone; CZM, Cohesive zone model; LEFM, Linear elastic fracture mechanics; TCZM, Trapezoidal Cohesive zone model; TSL, Traction separation law

any form of crack growth problem remains elusive. It is well appreciated in the literature that cyclic loading makes any crack propagation problem more complex, involving an unloading part of the loading cycle along with a process that is history dependent. The vast majority of crack propagation studies presented in the literature involving a CZM are limited to monotonic crack growth prediction. Therefore, in order to use the CZM for fatigue crack growth simulation, an irreversible and history-dependent cohesive law is required. Any such law must be able to account for and accommodate the damage accumulation associated with cyclic loading.[2] This can in principle be achieved by identifying additional criteria for the development of internal variables in any CZM thus providing history dependence. In the literature, there are two available models for identifying this cyclic history dependence, ie, the *envelope-load damage model* and the *loading-unloading hysteresis damage model*.

The maximum load of the loading cycle is the focus of the *envelope-load damage model* rather than a description of the complete cyclic loading behaviour. All variants founded on this particular approach formulate a damage rate dD/dN. Although the damage rate for convenience is written here in the form of a derivative, it should be well appreciated that the damage rate is not in fact a derivative as D is a path-dependent quantity and as such is not a function. The damage D is assumed composed of a quasi-static damage D^{s} and a cyclic damage D^{c}, which are considered to be additive to provide the total damage $D = D^{\mathrm{s}} + D^{\mathrm{c}}$. The damage accumulated $D_{(N\,+\,\Delta N)}$ is defined via the integration of damage rate. Thus, after a specific number of cycles, $N + \Delta N$ damage is determined from the current damage $D_{(N)}$ plus the integration of the damage rate over the interval $[N, N + \Delta N]$ and explicitly takes the form

$$D_{(N+\Delta N)} = D_{(N)} + \int_N^{N+\Delta N} (dD/dN)dN' \tag{1}$$

The integral in Equation (1) is typically approximated using 2-point Newton-Cotes quadrature; for example, in Robinson et al[3] and Tumino and Cappello,[4] the approximation takes the form

$$\int_N^{N+\Delta N} (dD/dN)dN' \approx \frac{1}{2}\left((dD/dN)|_N + (dD/dN)|_{N+\Delta N}\right)\Delta N \tag{2}$$

or alternatively with a 1-point Newton-Cotes quadrature as in previous studies,[5–10] which takes the form

$$\int_N^{N+\Delta N} (dD/dN)dN' \approx \left((dD^s/dN)|_N + (dD^c/dN)|_N\right) \tag{3}$$
$$\Delta N \approx \left(dD^c/dN\right)|_N \Delta N$$

A source of error in Equation (3) is the loss of the quasi-static damage rate, which cannot be estimated by means of the 1-point Newton-Cotes quadrature as explained in Bak et al.[11] Different formulations for the cyclic damage rate, found in the literature, are reviewed in Bak et al.[11] A fatigue CZM that can be applied for high cycle fatigue analysis of mode I, mode II, and mixed mode can be found in previous studies.[3,4,12,13] A particular concern with the damage rate equations adopted in these models is the number of material parameters involved, each requiring experimentation for their determination and for each loading mode. To reduce the cost required for calibrating parameters, the damage evolution can be linked to a Paris-like model as in other studies.[5-10] Linking damage evolution to a Paris-law means that no additional parameters require calibration other than the standard Paris-law parameter. Unfortunately, with this approach, predictive accuracy is affected since growth is confined by the particular growth law assumed to apply. Accuracy is also influenced by the integration scheme employed to integrate the damage rate equation. An additional contributory factor can be the absence of the component describing the quasi-static damage rate. Damage evolution can be directly related to the cohesive zone length (or at least to the fatigue part of the cohesive zone length). In literature,[5-10] for instance, the cohesive zone length is evaluated using

$$a^{\mathrm{cz}} = \frac{9\pi E_3 \mathcal{G}^{\mathrm{c}}}{32(\tau^{\circ})^2} \tag{4}$$

or a modified version of this equation, where a^{cz} is the cohesive zone length (the length of the process zone ahead of the crack tip where active cohesive elements are present), $\mathcal{G}^{\mathrm{c}}$ is the critical energy release rate, E_3 is Young modulus of the bulk material in the direction perpendicular to the crack plane, and τ° is the cohesive strength. The link to cohesive zone length in this way is essentially non-physical and consequentially cannot be measured or quantified experimentally.

Unlike the envelope-load approach, the entire loading-unloading cycle is considered and represented in *loading-unloading hysteresis damage models*. This permits the modelling of advanced behaviour at the cohesive interface and surroundings taking into consideration such things as friction and plasticity.[11] Loading-unloading hysteresis models are based on the reduction of the interfacial stiffness captured by a cyclic damage variable that evolves or an internal variable that grows; a review of CZMs for fatigue can be found in references herein.[14-17] The first successful attempt to use a CZM for the simulation of fatigue crack growth is presented in De-Andrés et al,[18] which introduces a cyclic damage

variable D, whose purpose is to quantify the amount of dissipated energy in the fracture process divided by the critical fracture energy. Variable interfacial stiffness models soon followed this work (see Nguyen and Repetto[19] and Yang et al,[20] for example), where traction rate $\dot{T}$ is assumed to be a function of incremental stiffnesses K^- and K^+ according to the relationship,

$$\dot{T} = \begin{cases} K^-\dot{\delta}, & if \ \dot{\delta} < 0 \\ K^+\dot{\delta}, & if \ \dot{\delta} > 0 \end{cases} \tag{5}$$

where K^+ and K^- are loading and unloading stiffness, respectively, and $\dot{\delta}$ is the rate of change of separation.

A particular deficiency with these models is that crack defects are assumed to grow no matter how small they might be, which can be an unrealistic behaviour. To correct for this, introduced in Roe and Siegmund[21] are two additional parameters σ^f and δ^Σ that represent the endurance limit and the accumulated cohesive length, respectively. If the component of stress normal to the crack at the element ahead of the crack tip is less than the endurance limit, then the model presents an infinite life (no crack will propagate). Although this model contains the basic features necessary for describing fatigue crack growth, like all previous models, it remains phenomenological requiring validation with experimental results to check accuracy and to standardise the cohesive zone parameters. Other studies[17,22-24] have considered similar approaches. Although the loading-unloading hysteresis damage model replicates to an extent, fatigue behaviour over each and every time increment, it is rather costly in terms of computational time, and from a practical viewpoint, it is unfeasible for high cycle fatigue simulation, where analysis can typically involve extremely large numbers of loading cycles.

To overcome the cost associated with hysteresis damage models, De-Andrés[18] introduced an extrapolation scheme to estimate the damage state after a specific number of cycles by a two-term Taylor expansion of the form

$$D_{n+1} \approx D_n + (dD/dN)|_n (N_{n+1} - N_n) \tag{6}$$

The rate of change of D per cycle dD/dN at N_n, required for the extrapolation, is computed by a detailed step-by-step computation of a few loading cycles. A limitation of this method is the assumption that the damage rate is constant throughout the crack propagation period. In addition, for good accuracy, the cycle increment $N_{n+1} - N_n$ is constrained by the requirement that the damage increment $D_{n+1} - D_n$ is relatively small. Similar methods are considered in Towashiraporn et al[25] and Koutsourelakis et al.[26]

In general, fatigue modelling using the CZM looks very promising but is still in its infancy with no mature CZMs yet available for use in industrial applications.[11] However, in an attempt to advance the approach, this paper introduces a loading-unloading hysteresis damage model containing a fast-track feature.

The new CZM is introduced in Section 2 along with the fast-track feature and a mechanism for capturing irreversibility. The implementation of the new CZM model in the commercial software package ABAQUS (via a bespoke UMAT subroutine) is discussed in Section 3. In addition, the analysis model properties (geometry, material properties, and boundary conditions) along with a mesh-sensitivity analysis are considered. Section 4 focuses on the validation of the new model by presenting, discussing, and comparing results with experimental fatigue data. Conclusions are presented in Section 5.

2 | COHESIVE ZONE MODEL FOR FATIGUE

The fracture process can be simplified to the form shown in Figure 1, where the behaviour of the material element at the crack tip is assumed to follow a predefined traction separation law (TSL). Different forms of TSLs used in the literature include polynomial, exponential, bilinear, and trapezoidal shapes as shown in Figure 2. A cohesive model is not physical but phenomenological and attempts to represent the physics of the fracture process by means of a single separating interface. Therefore, there is no physical evidence for the shape of the function that relates traction to separation. The effect of the traction-separation law shape is discussed in Tvergaard and Hutchinson,[27] where it is concluded that the shape of

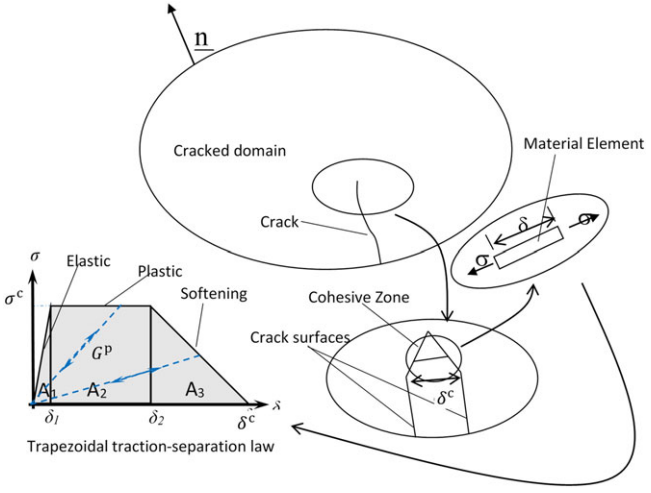

FIGURE 1 Mode I cohesive zone model[28] [Colour figure can be viewed at wileyonlinelibrary.com]

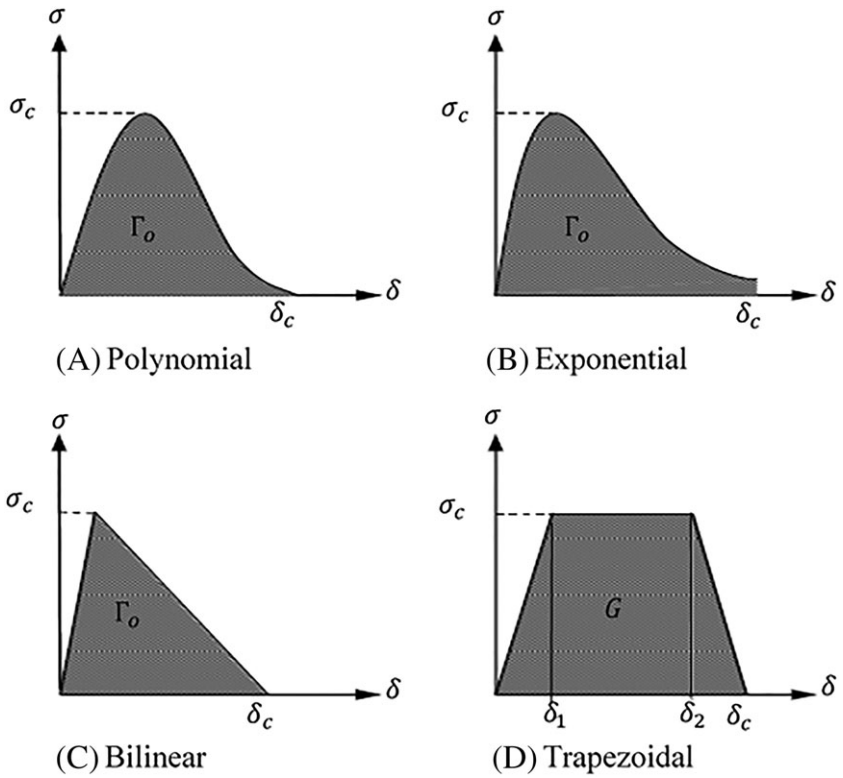

FIGURE 2 The widely used traction separation laws: (A) polynomial, (B) exponential, (C) bilinear, and (D) trapezoidal[29]

the law does not significantly affect the analysis results. However, it is shown in previous studies[28,30-32] that the TSL has an effect on fracture behaviour but the significance of this effect depends on geometry and material properties.

For a pre-defined TSL, two of the cohesive parameters (I^{o}, σ^{c}, and δ^{c}) are usually sufficient for simulating the fracture process, where I^{o} is the energy dissipated in the formation of new surfaces, σ^{c} is the critical cohesive traction, and δ^{c} is the critical cohesive separation at which the cohesive element fails. The trapezoidal cohesive zone model (TCZM) on the other hand involves an additional shape parameter (δ_2), which is required to be specified to simulate the complete fracture process. The addition of this parameter is to account for local plasticity at the crack tip, so avoiding the need for a global elastic-plastic analysis in a situation where only localised plasticity is involved. This feature is advantageous computationally as it permits an elastic-bulk material to be assumed. The area under the traction curve represents the total dissipated energy (G^{c}) (ie, the plastic energy dissipated in the local plastic zone and the energy required to form new surface), which is represented mathematically as

$$G^{c} = \int_0^{\delta^{c}} \sigma_{(\delta)} d\delta \tag{7}$$

which for a trapezoidal cohesive model depicted in Figure 1, gives

$$\begin{aligned} G^{c} &= \left(\int_0^{\delta_1} \sigma_{(\delta)} d\delta + \int_{\delta_2}^{\delta^{c}} \sigma_{(\delta)} d\delta\right) + \int_{\delta_1}^{\delta_2} \sigma_{(\delta)} d\delta \\ &= (A_1 + A_3) + A_2 = \Gamma^{o} + G^{p} \\ &= \left(\frac{\sigma^{c}}{2}\delta_1 + \frac{\sigma^{c}}{2}(\delta^{c} - \delta_2)\right) + \sigma^{c}(\delta_2 - \delta_1) \\ &= \frac{\sigma^{c}}{2}(\delta_2 - \delta_1 + \delta^{c}) \end{aligned} \tag{8}$$

where G^{c} is the total dissipated energy per unit area, G^{p} is the local plastic dissipated energy, δ_1 is the separation at which the deformation become permanent, and δ_2 is the separation at which the element deterioration is assumed to start.

The standard TCZM is represented mathematically as

$$\sigma_{(\delta)} = \begin{cases} K^{coh}\delta & \text{if } \delta < 0 \\ K\delta & \text{if } 0 \le \delta \le \delta^{max} \\ \sigma^{c} & \text{if } \delta^{max} < \delta < \delta_2 \\ \left(1 - D_{(\delta)}\right)\sigma^{c} & \text{if } \delta_2 < \delta^{max} < \delta < \delta^{c} \\ 0 & \text{if } \delta \ge \delta^{c} \end{cases} \tag{9}$$

where $\sigma_{(\delta)}$ is the cohesive traction and $K^{coh} = \sigma^{c}/\delta_1$, which represents the cohesive stiffness of an undamaged cohesive element. Similarly, K is the cohesive stiffness of a damaged cohesive element (which initially equals K^{coh}) and is defined by

$$K = \frac{\sigma^{max}}{\delta^{max}} \tag{10}$$

where δ^{max} and σ^{max} are the separation and stress at the onset of unloading; these initially take the values δ_1 and σ^c, respectively, to ensure $K = K^{coh}$ if no damage is present in the cohesive element.

Note that for the standard TCZM at unloading, the crack is fully closed and the cohesive traction is returned to zero following the relationship $\sigma_{(\delta)} = K\delta$ (the model does not account for crack closure). The subsequent reloading follows the same path as illustrated in Figure 1. As advised by Scheider et al,[33] the value of δ_1 should be very small and the value of δ_2 should be close to δ^c. Therefore, in this study, these values are set to

$$\delta_1 = \frac{\sigma^c}{K^{coh}} \tag{11}$$

$$\delta_2 = 0.75 \times \delta^c \tag{12}$$

The damage process is assumed to be void initiation, growth, and coalescence, which is represented by the parameter $D_{(\delta)}$ in the cohesive model. For the TCZM, the damage variable can be represented by the relationship

$$D_{(\delta)} = 1 - \frac{(\delta^c - \delta)}{(\delta^c - \delta_2)} \qquad \text{if } \delta_2 \le \delta \le \delta^c \tag{13}$$

which has the rate form $\dot{D}_{(\delta)} = F_{(\delta)}\dot{\delta}$, where $F_{(\delta)}$ is a positive function of the form

$$F_{(\delta)} = \frac{1}{(\delta^c - \delta_2)} \tag{14}$$

and as above, rate is conveniently represented symbolically here, in the form of a derivative, ie, $\dot{D}_{(\delta)} = dD_{(\delta)}/dN$ and $\dot{\delta} = d\delta/dN$.

If cyclic loading is applied, the standard TCZM will result in an infinite life. Therefore, it is necessary to use an irreversible and history-dependent CZM in order to capture finite life. This can be done by identifying a cyclic damage mechanism.

2.1 | Fatigue cohesive model

The damage mechanism used for the new TCZM consists of two parts. First is the cyclic damage D^c, which itself is associated with two distinct effects: (1) an increase in local plastic separation δ^p when $\delta \le \delta_2$ and (2) for $\delta > \delta_2$, a further increase in δ^p as consequence of void growth and coalescence. Second is monotonic damage D^s that results from material deterioration not attributed to cyclic loading in the CZM. These two features are shown to be sufficient for the TCZM to capture fatigue crack growth.

A schematic outline of the behaviour of the proposed model is presented in Figure 3, with traction represented mathematically by

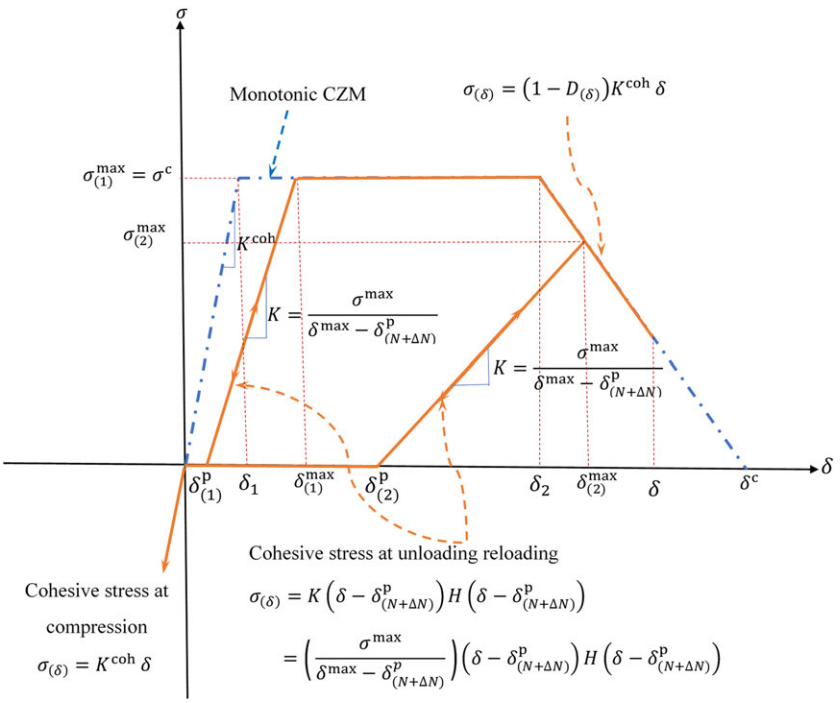

FIGURE 3 New loading-unloading hysteresis model [Colour figure can be viewed at wileyonlinelibrary.com]

$$\sigma_{(\delta)} = \begin{cases} K^{\text{coh}}\delta & \text{if } \delta < 0 \\ \left(\dfrac{\sigma^{\max}}{\delta^{\max} - \delta^{\text{p}}}\right)(\delta - \delta^{\text{p}})H(\delta - \delta^{\text{p}}) & \text{if } 0 \le \delta \le \delta^{\max} \\ \sigma^{c} & \text{if } \delta^{\max} < \delta < \delta_2 \\ \left(1 - D_{(\delta)}\right)\sigma^{c} & \text{if } \delta_2 < \delta^{\max} < \delta < \delta^{c} \\ 0 & \text{if } \delta \ge \delta^{c} \end{cases} \tag{15}$$

where in this model, the critical cohesive stress σ^{c} doubles up as the endurance limit, which is the stress level required for activating the damage accumulation mechanism; loads resulting in stresses below σ^{c} in the cohesive zone will result in an infinite life. The Heaviside function H is defined to zero when δ is smaller than δ^{p} and one in other cases. Finally, $D_{(\delta)}$ is the damage variable of Equation (13). The separation δ has two parts, ie,

$$\delta = \delta^{p} + \delta^{cyc} \tag{16}$$

where δ^{cyc} is the cyclic separation as a result of the applied load at any time increment, with plastic separation δ^{p} updated by means of integration of a rate relationship, ie,

$$\delta^{\text{p}}_{(N+1)} = \delta^{\text{p}}_{(N)} + \int_{N}^{N+1}\left(d\delta^{\text{p}}_{(N')}/dN\right)dN' \tag{17}$$

where $\delta^{\text{p}}_{(N)}$ is the stored plastic separation from the previous loading cycle and $d\delta^{\text{p}}_{(N)}/dN$ is the rate of change in plastic separation (represented here in the form of a derivative for convenience), ie, the increase in the plastic separation δ^{p} per cycle.

The integral in Equation (17) can be approximated using the mean value theorem for integration. If $d\delta^{\text{p}}_{(N)}/dN$ is assumed to be defined and smooth on the interval $(N, N+1)$, then

$$\begin{aligned} \int_{N}^{N+1}\left(d\delta^{\text{p}}_{(N')}/dN\right)dN' &= (N+1-N) \times \left(d\delta^{\text{p}}_{(N)}/dN\right)_{(\alpha)} \\ &= \left(d\delta^{\text{p}}_{(N)}/dN\right)_{(\alpha)} \end{aligned} \tag{18}$$

where α belongs to the interval $[N, N+1]$ and $\left(d\delta^{\text{p}}_{(N)}/dN\right)_{(\alpha)}$ is an intermediate value of the rate $d\delta^{\text{p}}_{(N)}/dN$, which in this work is assumed to be proportional to the maximum separation $\delta^{\text{cyc}^{\max}}$, reached at the end of a loading cycle. This assumption provides a convenient approximation of the form,

$$\left(d\delta^{\text{p}}_{(N)}/dN\right)_{(\alpha)} \approx \frac{\delta^{\text{cyc}^{\max}}}{C} \tag{19}$$

where C is a positive dimensionless constant of proportionality and takes a value greater than unity to reflect the fact that only a proportion of $\delta^{\text{cyc}^{\max}}$ contributes to plastic separation.

Note that the origin of Equation (19) is a rate equation of the form $\dot{\delta^{p}} = h(\delta^{\text{cyc}})$, where h is a positive function. The exact form the function h takes is not important here since the approximation adopted in Equation (19) is sufficient and expedient since $\delta^{\text{cyc}^{\max}}$ is dependent on the loading conditions (to account for the loading history) with any material cyclic damage being readily captured by the material parameter C, which can be tuned to accommodate particular material behaviour on comparing analysis results with experimental data. The dimensionless parameter C provides an indication of the rate at which plastic separation is taking place in a material and consequently is material dependent. It is however independent of the specimen shape and loading conditions and once determined for a particular material can in principle be applied to any loading case. Substitution of Equation (19) into Equation (17) yields an extraordinarily simple increment rule for cyclic damage, ie,

$$\delta^{\text{p}}_{(N+1)} \approx \delta^{\text{p}}_{(N)} + \frac{\delta^{\text{cyc}^{\max}}}{C} \tag{20}$$

Shown in Figure 4A is the behaviour of the cohesive model under cyclic loading, and the accumulated dissipated energy ΔG is readily shown to be

$$\Delta G = \begin{cases} \dfrac{1}{2}[\sigma^{c}(\delta^{\max} + \delta^{\text{p}} - \delta_1)] & \text{if } \delta^{\max} \le \delta_2 \\ \dfrac{1}{2}[\sigma^{c}(\delta^{\max} + \delta_2 - \delta_1) - \sigma^{\max}(\delta_2 - \delta^{\text{p}})] & \text{if } \delta^{\max} > \delta_2 \end{cases} \tag{21}$$

represented by the area under the traction-separation curve in Figure 4.

2.2 | Fast-track feature

The model described in Section 2.1 can be shown to represent fatigue behaviour but suffers from a particular limitation. In its present form (similar to the loading-unloading hysteresis damage model), it is practically unfeasible and computationally costly requiring excessively long computational time as a consequence of the large numbers of cycles typically involved in any realistic industrial application. In order to overcome this particular limitation, it is necessary to find an approach that limits the extent of the computational requirements. An observation of the behaviour of the existing model however is that deviation in the cyclic behaviour tends to evolve extremely slowly. Cyclic damage is considered

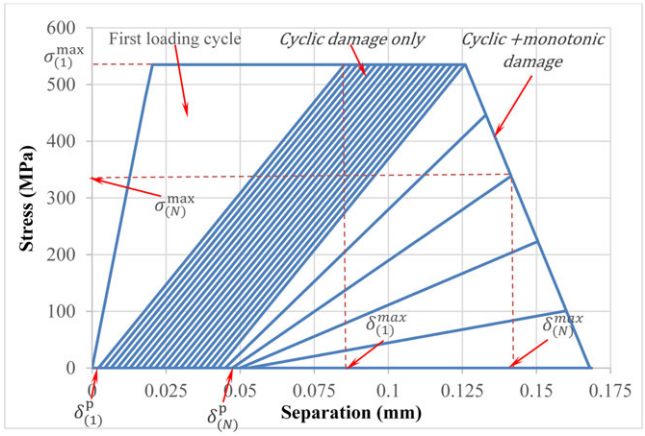

(A) Cycle by cycle

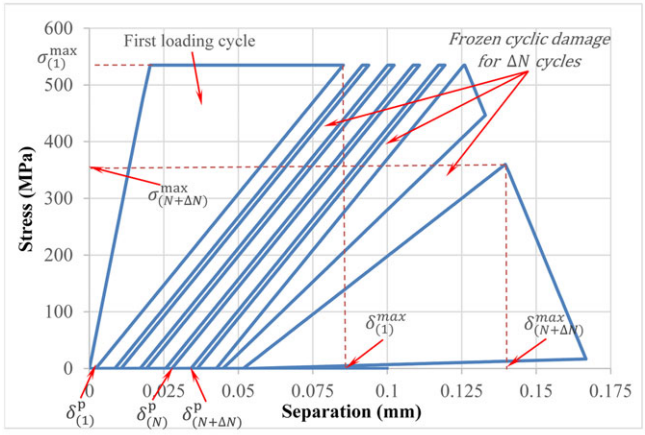

(B) Fast-track procedure with $\Delta N = 4$

FIGURE 4 Cyclic stress-separation curves [Colour figure can be viewed at wileyonlinelibrary.com]

here to be a combination of cyclic plastic separation and material deterioration, and it is the cyclic plastic separation that is observed to suffer low cyclic deviation. This suggests that a reasonable approximation is a linear growth rule for cyclic plastic separation with constant plastic increment over a specific load envelope containing ΔN cycles. This simple observation provides the founding idea for the new fast-track procedure.

Consider then the possibility that the rate of change in cyclic plastic separation evaluated in a loading cycle remains constant for a specific load envelope containing ΔN number of cycles; the value of ΔN should not be set at a value too high to allow damage to be updated to maintain accuracy. The cyclic plastic separation after $(N + \Delta N)$ is evaluated in the usual way as

$$\delta^{\mathrm{p}}_{(N+\Delta N)} = \delta^{\mathrm{p}}_{(N)} + \int_{N}^{N+\Delta N} \left(d\delta^{\mathrm{p}}_{(N')} / dN \right) dN' \qquad (22)$$

Similar to Equation (17), the integral in Equation (22) is approximated using the mean value theorem for integration and on applying the approximation in Equation (19), the cyclic plastic separation after $(N + \Delta N)$ cycles is approximated as

$$\delta^{\mathrm{p}}_{(N+\Delta N)} \approx \delta^{\mathrm{p}}_{(N)} + \left(\frac{\delta^{\mathrm{cyc^{max}}}}{C} \right) \Delta N \qquad (23)$$

where Equation (20) is returned on setting $\Delta N = 1$.

The increment ΔN for computational expediency can be any integer value significantly greater than one, but accuracy is a limiting consideration. It is important therefore to have some understanding about the effect ΔN has on the accuracy of the fast-track procedure. A simple procedure (not connected to fatigue analysis per se) is adopted for the sole purpose to provide a reasonable estimate for the value of ΔN, which involves first the analysis of one cycle. From this cycle, information is recovered at the integration point (IP) at the crack tip, with ΔN being set by the relationship,

$$\Delta N = \mathrm{int} \left(\frac{\delta^{\mathrm{c}} - \delta^{\mathrm{cyc^{max}}}}{N^{u} \times \delta^{\mathrm{p}}_{(1)}} \right) \qquad (24)$$

where int is a function that returns the nearest integer to the argument, N^{u} is a parameter that represents the number of required updates of the cyclic damage, $\delta^{\mathrm{p}}_{(1)}$ is the cyclic plastic separation after the first loading cycle, and $\delta^{\mathrm{cyc^{max}}}$ and δ^{c} are the maximum cyclic separation reached at the loading cycle and the critical cohesive separation, respectively. The numerator $\delta^{\mathrm{c}} - \delta^{\mathrm{cyc^{max}}}$ in Equation (24) is a relatively crude approximation of the cyclic plastic separation to the point of failure. The ratio of $\delta^{\mathrm{c}} - \delta^{\mathrm{cyc^{max}}}$ and $\delta^{\mathrm{p}}_{(1)}$ gives an indication of the number of cycles that leads to the failure of the IP at the crack tip. The value for ΔN employed as a cyclic load envelope is obtained on dividing $\left(\delta^{\mathrm{c}} - \delta^{\mathrm{cyc^{max}}}\right) / \delta^{\mathrm{p}}_{(1)}$ with the integer N^{u} (representing the number of cyclic updates deemed necessary for accuracy) and returning the nearest integer. The greater the value of N^{u}, the lower the value of ΔN (with $\Delta N \geq 1$) but consequently the greater the computational cost.

The predicted value of ΔN by Equation (24) is estimated in a one cycle analysis, and the final value is applied as a fixed input to all the cohesive elements in the fatigue analysis along with (σ^{c}, δ^{c}, and C) for all cohesive elements. The value of ΔN (with N^{u} fixed) will automatically be higher if the problem under consideration involves high cycle fatigue since both the maximum cyclic separation and the cyclic plastic increment will be smaller. A detailed investigation on the effect of ΔN on the simulation results is provided in Section 3.3.

The separation δ^{max} and the stress σ^{max} at the end of the $N + \Delta N$ cycles are determined with

$$\delta^{max} = \delta^{p}_{(N+\Delta N)} + \delta^{cyc^{max}} \tag{25}$$

$$\sigma^{max} = \begin{cases} \sigma^{c} & \text{if } \delta_1 < \delta^{max} \le \delta_2 \\ \left(1 - D_{(\delta^{max})}\right) \times \sigma^{c} & \text{if } \delta_2 < \delta^{max} \le \delta^{c} \end{cases} \tag{26}$$

Thus, after $N + \Delta N$ cycles, Equation (26) returns the maximum stress, which is equal to the cohesive critical stress if δ^{max} (from Equation (25)) is less than δ_2. If, however, δ^{max} is larger than δ_2, then the maximum stress σ^{max} is evaluated in a similar fashion to Equation (15), by using the monotonic damage variable $D_{(\delta^{max})}$ of Equation (13), with δ replaced by δ^{max}. The evaluated values from Equations (25) and (26) are provided to the next loading cycle along with the new value of δ at $N + \Delta N$, with δ determined using Equation (16) and applied in Equation (15).

To keep things reasonably simple, ΔN is assumed to remain invariant for the total process. To record the exact number of cycles when the cohesive element fails and bearing in mind that at the end of a loading cycle, the number of cycles satisfies the relationship $N_{i+1} = N_i + \Delta N$, it is necessary to compare the value of δ^{max} (evaluated by using Equation (25)) with δ^{c}, and if larger, then the number of cycles at which the element failed satisfies the relationship

$$N^{f} = N_{i+1} - \text{int}\left(\frac{\delta^{max} - \delta^{c}}{\left(\delta^{cyc^{max}}/C\right)}\right) \tag{27}$$

The second term on the right-hand side of Equation (27), represents the unwanted number of cycles that do not contribute to failure. The numerator $\delta^{max} - \delta^{c}$ represents the cyclic damage as a result of this unwanted number of cycles, with the denominator $\delta^{cyc^{max}}/C$ being cyclic damage increment. The ratio of $\delta^{max} - \delta^{c}$ and $\delta^{cyc^{max}}/C$ therefore provides an estimation of the overshoot in the prediction of the number of cycles to failure and hence must be removed as shown in Equation (27).

3 | IMPLEMENTATION OF THE NEW CZM IN ABAQUS

The commercial finite element solver ABAQUS is used as a vehicle for the numerical analysis in this study. In ABAQUS, the fracture process using the cohesive model can be identified either by a cohesive surface or by cohesive elements that are situated along the crack path. In this study, cohesive elements are used although existing elements in ABAQUS are somewhat constrained by TSLs that are history independent and not applicable for the simulation of fatigue crack growth. However, the TSL can be defined through their material behaviour, and ABAQUS provides a facility to specify new material behaviour (as the new cohesive model introduced in this study) through a user-defined material subroutine.

3.1 | UMAT implementation and testing

To test the UMAT subroutine, a three-element model (two continuum elements and one cohesive element connecting them) is used as shown in Figure 5. The material properties in the bulk material and the cohesive element are shown in Table 1. The parameter C is set to have a small value (ie, 40) to artificially reduce the number of cycles required for failure of the cohesive element. The load is applied as a cyclic displacement with fixed maximum amplitude of 11.6×10^{-5} m and $R = 0$. The analysis is performed initially on a cycle-by-cycle basis (ie, $\Delta N = 1$) and then with the new fast-track technique on setting $\Delta N = 4$. The cyclic stress of the new fatigue

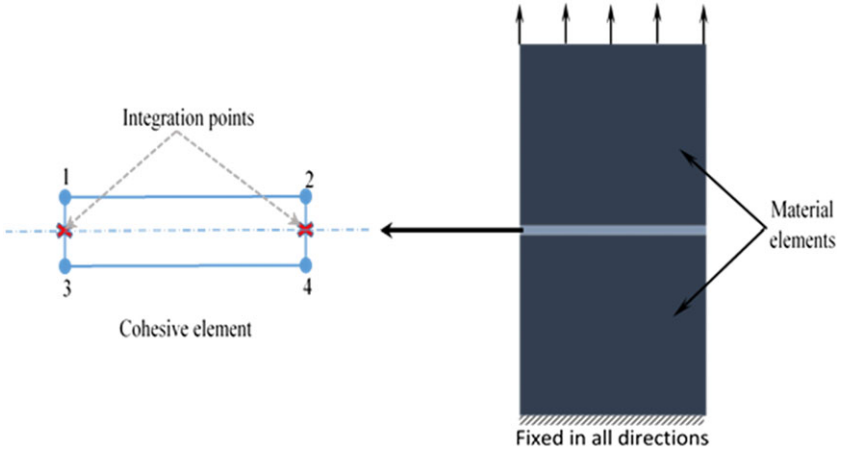

FIGURE 5 Implementation of the cohesive element in the finite element model [Colour figure can be viewed at wileyonlinelibrary.com]

TABLE 1 Material properties

Bulk Material	σ^Y, MPa	E, GPa	ϑ				
	340	193	0.29				
Cohesive elements	Γ^o, N/m	K^{coh}, GPa/m	σ^c, MPa	δ^c, mm	δ_1, mm	δ_2, mm	C
	68 500	19 700	511	0.168	0.025 94	0.126	40

model (in a cycle-by-cycle manner first and by using the new technique with $\Delta N = 4$) is shown with respect to the separation and time in Figures 4 and 6, respectively. The graphs shown in Figure 4 reveal how the model can readily cater for an initially high load resulting in a correspondingly high level of energy dissipation and monotonic damage apparent in the first cycle. This is then followed by cyclic damage at significantly lower levels of dissipation per cycle. Also shown in Figure 4 is the growth of the plastic separation with the number of cycles until the separation δ reaches δ_2; at which point, the cohesive stiffness decreases with increasing number of cycles because of material deterioration leading to failure of the cohesive element. The required analysis time for a typical element to fail using the cycle-by-cycle model (dashed curve) and the fast-track model (solid curve) is shown in Figure 6. It reveals that the fast-track procedure provides a reduced number of cycles and hence computational effort, which of the order of ΔN^{-1} of that required without its implementation. The figure shows that for an analysis involving 26 loading cycles, the fast-track procedure takes some 140 seconds while the cycle-by-cycle analysis takes 560 seconds.

3.2 | Analysis model: Geometry and boundary conditions

The finite element model depicted in Figure 7 conforms to the shape of the specimens used in the fatigue experimental trials. The numerical model consists of 23 618 plane-stress elements of which 22 988 (type CPS4), 390 (type CPS3), and 240 cohesive elements (type COH2D4).[34] The material properties for the bulk material element and the cohesive element are found in Table 2.

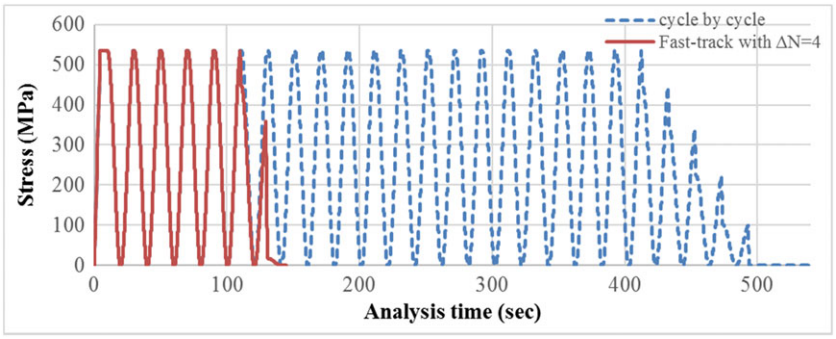

FIGURE 6 Cyclic stress as a function of time [Colour figure can be viewed at wileyonlinelibrary.com]

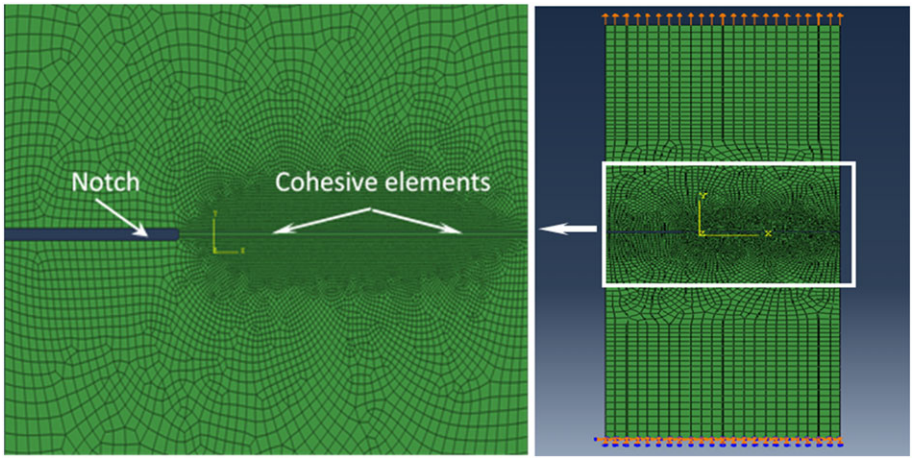

FIGURE 7 Boundary conditions and loading for finite element model [Colour figure can be viewed at wileyonlinelibrary.com]

TABLE 2 Material properties full model

Bulk material	σ^{Y}, MPa	E, GPa	ϑ				
	340	193	0.29				
Cohesive elements	Γ^{o}, N/m	K^{coh}, GPa/m	σ^{c}, MPa	δ^{c}, mm	δ_1, mm	δ_2, mm	C
	47 039	19 700	340	0.168	0.017 26	0.126	775

The initial values of the cohesive parameters were set as follows: δ^{c} equals the crack tip opening displacement (CTOD) as measured experimentally in a CT specimen and equals 0.000 168 m; the value of the critical cohesive stress was set to equal the material yield stress, and its value is 340 MPa.

The new fatigue algorithm is initiated with a cycle-by-cycle analysis with these initial values for a few hundred cycles to determine the correct value of the parameter C, which is obtained by means of curve fitting analysis results and contrasting with experimentally obtained fatigue data. The final value of C is subsequently used in a one cycle analysis to obtain an optimum value of ΔN, which is chosen to provide good accuracy for a substantially reduced computational effort. In the present model, the selected value of ΔN is applied over the full fatigue analysis; the parameter set in Table 2 was found to give the best fit.

The boundary conditions applied to the analysis model are shown in Figure 7. Loading is in the form of a uniform cyclic displacement in the y-direction applied at the top surface and fixed in all directions at the bottom surface. The load is applied in 20 steps: first, a ramp load that increases from zero to 3.65×10^{-5} m followed by 19 steps with sinusoidal load at $R = 0$ and maximum displacement of (7.3, 7.6, 7.8, 8, 8.2, 8.4, 8.5, 8.6, 8.7, 9, 9.2, 9.6, 10, 10.2, 10.4, 11.2, 12, 15.2, 20.6)$\times 10^{-5}$ m, respectively, as shown in Figure 8. The number of cycles in each step is 6400, 3200, 2400, 1600, 1600, 1600, 1600, 1600, 1600, 800, 800, 800, 800, 800, 800, 800, 800, 800, 800 (the last step is run until failure), respectively. The number of cycles at each step is set to ensure that the loading conditions match to those of the fatigue experiment.

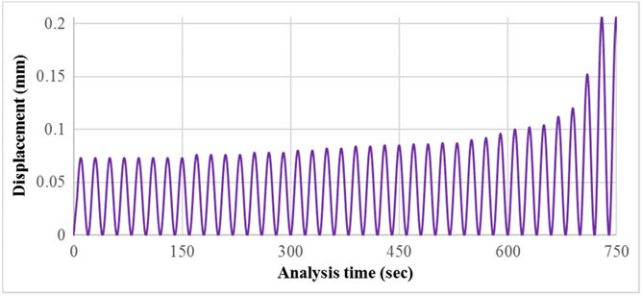

FIGURE 8 Load as a function of time [Colour figure can be viewed at wileyonlinelibrary.com]

3.3 | Fast-track effect on accuracy of the result

The effect of the updates parameter N^{u} found in Equation (24) (and consequently ΔN) on the damage variable and the dissipated energy as tested on the three-element model is shown in Table 3 and Figures 9 and 10, and its effect on the crack growth on full model is shown in Figures 11 and 12. In general, a decrease in the value of N^{u} (increasing the value of ΔN) gives rise to a predicted slower crack growth. From Table 3, the error in the estimated number of cycles at failure and the value of the damage variable D is found to be dependent on the value of N^{u}, since for $\Delta N = 2$ (ie, $N^{u} = 12$), the error is 0% while for $\Delta N = 3$ (ie, $N^{u} = 8$), the error in the predicted result is 4%. The error in the simulation results becomes significant when N^{u} is set to a small value, for example, the error in the case when $\Delta N = 10$ (ie, $N^{u} = 2$) is 24%. The results indicate the expected behaviour where greater values of N^{u} (and hence lower values of ΔN) lead to a reduction in observable differences. From Table 3 and Figures 9 and 10, it is observable that there is little dependence of the results on the value of ΔN in the virtual-plastic region (ie, when $\delta^{max} \leq \delta_2$). However, differences become more noticeable in the region of material deterioration (ie, $\delta^{max} > {}_2$). However, revealed in Figure 10 is that acceptable results are achievable if ΔN is such that the damage is updated reasonably regularly (ie, N^{u} is not too low). From the results shown in Figures 11 and 12, it can be concluded that any value higher than 6 for the updates parameter N^{u} provides satisfactory results with a significant reduction in computational cost. It is clear from Figure 11 that the predicted results are reasonably close to each other for values of N^{u} set to (56, 28, 14, 7), which correspond to $\Delta N \approx (100, 200, 400, 800)$, respectively. Differences are more noticeable however for values of N^{u} lower than 6, where $N^{u} = 3$ corresponds to $\Delta N \approx 2000$ and $N^{u} = 1$ corresponding to $\Delta N \approx 5600$, as shown in Figure 12. In this study, a value of $N^{u} = 7$ corresponding to $\Delta N \approx 800$ was found to be sufficient for good accuracy and a significant reduction in numerical analysis time. The analysis of the problem under consideration took just few hours on a PC platform with $N^{u} = 7$ ($\Delta N = 800$). The ratio of CPU time with the fast-track procedure over the

TABLE 3 Local effect of ΔN on the damage variable D and the dissipated energy ΔG(three-element model)

	$\Delta N = 1$			$\Delta N = 2$			$\Delta N = 3$			$\Delta N = 6$			$\Delta N = 10$		
N	δ^{max}, mm	ΔG, kN/m	D	δ^{max}, mm	ΔG, kN/m	D	δ^{max}, mm	ΔG, kN/m	D	δ^{max}, mm	ΔG, kN/m	D	δ^{max}, mm	ΔG, kN/m	D
1	0.0852	16.8	0	0.0852	16.8	0	0.0852	16.8	0	0.0852	16.8	0	0.0852	16.8	0
3	0.0895	18.9	0			0	0.0895	18.9	0						
6	0.0959	22.1	0	0.0959	22.1	0	0.0959	22.1	0	0.0959	22.1	0			
9	0.102	25.3	0			0	0.102	25.3	0						
10	0.104	26.4	0	0.104	26.4	0			0				0.104	26.4	0
12	0.109	28.5	0	0.109	28.5	0	0.109	28.5	0	0.109	28.5	0			
15	0.115	31.7	0			0	0.115	31.7	0						
18	0.121	34.9	0	0.121	34.9	0	0.121	34.9	0	0.121	34.9	0			
20	0.126	37.0	0	0.126	37.0	0							0.126	37.0	0
24	0.160	63.0	0.81	0.160	57.7	0.81	0.146	53.1	0.48	0.134	45.0	0.19			
25	Failed	68.5	1	Failed	68.5	1									
26							Failed	68.5	1						
27										Failed	68.5	1			
30													0.153	59.4	0.64
31													Failed	68.5	1

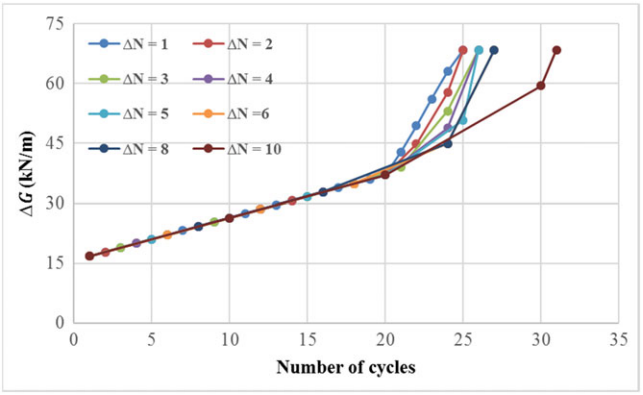

FIGURE 9 Dissipated energy with the number of cycles as a function of ΔN applied on the three-element model [Colour figure can be viewed at wileyonlinelibrary.com]

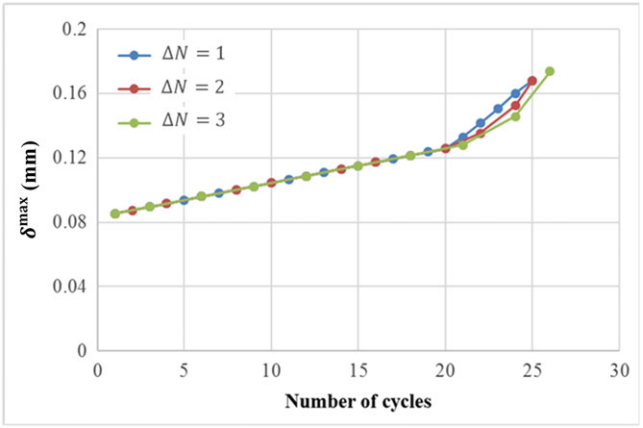

FIGURE 10 Change in δ^{max} with the number of cycles for three values of ΔN applied on the three-element model [Colour figure can be viewed at wileyonlinelibrary.com]

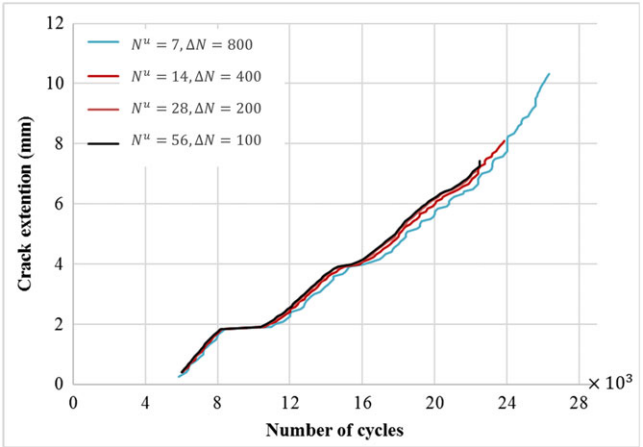

FIGURE 11 Crack length prediction for reasonable values of N^u at $R = 0$ and a frequency of 0.05 Hz [Colour figure can be viewed at wileyonlinelibrary.com]

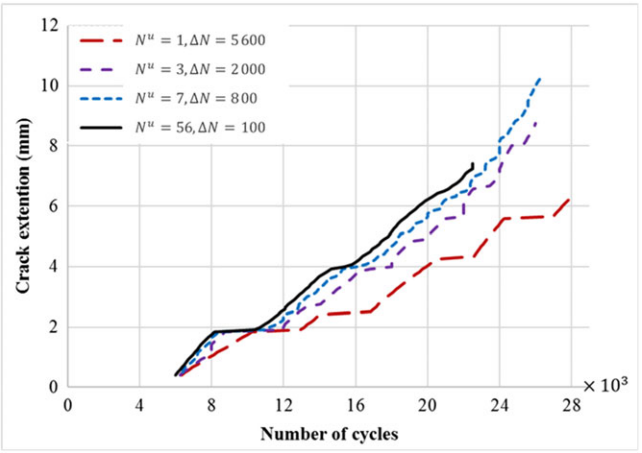

FIGURE 12 Crack length prediction for relatively small values of N^u at $R = 0$ and a frequency of 0.05 Hz [Colour figure can be viewed at wileyonlinelibrary.com]

CPU-time with the cycle-by-cycle analysis is of the order of ΔN^{-1}.

3.4 | Mesh sensitivity analysis

Converged results have been confirmed by running a mesh sensitivity analysis. Increasing the overall number of bulk-material elements or the cohesive zone elements has been found to have little impact on the results presented. However, it might be well anticipated that the number of elements in the cohesive zone will be critical to a good outcome. The length of the cohesive zone represents the distance between the actual crack tip and the analytical crack tip. This zone includes the active cohesive elements, and it directly linked to the crack-tip plastic zone, so its length can be estimated through a similar formulation to the plastic zone estimated by von Mises yield criterion as

$$l^{\text{coh}} = \frac{E\ G^{\text{c}}}{2\pi(\sigma^{\text{c}})^2}. \tag{28}$$

For the problem under consideration, the length of the cohesive zone is 8.4 mm, whereas the length of the ligament is 20 mm. It is possible to deduce from the plots shown in Figure 13 that the number of cohesive elements in the cohesive zone only has a minor influence on the crack growth and fatigue life. However, if the focus is to accurately represent the stress field at the crack tip, a higher number of elements is required (see Figure 14). In this work, 101 cohesive elements in the cohesive zone are employed to ensure that numerical errors are insignificant.

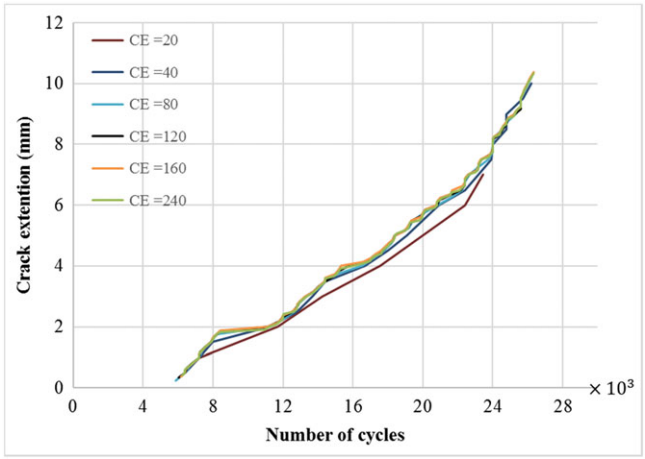

FIGURE 13 Importance of the number of cohesive elements in the cohesive zone [Colour figure can be viewed at wileyonlinelibrary.com]

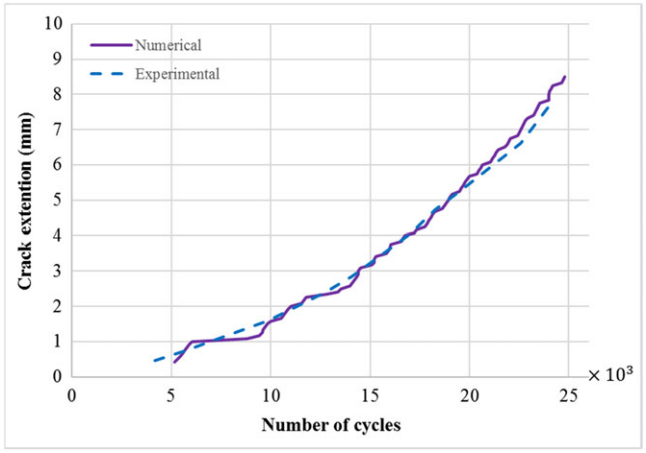

FIGURE 15 Numerical prediction (at $\sigma^c = 340$ MPa, $C = 775$, $N^u = 7$, $R = 0$, and $f = 0.05$ Hz) versus experiment (at $R = 0$ and $f = 0.05$ Hz) [Colour figure can be viewed at wileyonlinelibrary.com]

4 | RESULTS AND DISCUSSION

To overcome the inherent limitations of the loading-unloading hysteresis damage model, a new CZM with fast-track facility has been introduced. This model is founded on the basis of loading-unloading hysteresis but with the facility to "freeze in" damage for a loading cycle over a predefined number of cycles. The damage is updated in the next loading cycle to comply with the conditions at the new state at $N + \Delta N$ cycles. The approach has been proven to be efficient in terms of time and computational cost reduction. Analyses that can require months or possibly years to be solved (depending of the computational platform) using a cycle-by-cycle approach can be resolved in just a few hours or few days to a good accuracy. Shown in Figure 15 is experimental and predicted crack length versus the number of cycles; although the crack growth curve predicted with the new approach (with $\Delta N \approx 800$) shows a delay in crack initiation and a temporary crack arrest at the early stages of crack growth, the overall predicted crack propagation is in good agreement with the experimental data. The deviant behaviour at crack initiation is as a consequence of the time required to fully develop a stable cohesive zone as shown in Figure 15. The cohesive model in this sense differentiates between a virgin crack and a crack developed through fatigue.

One advantage of the new model over the previous models proposed in literature[18,25,26,35] is its simplicity. The model does not require the establishment of a relationship that links the damage to the number of cycles as in previous work. The damage in this case is calculated

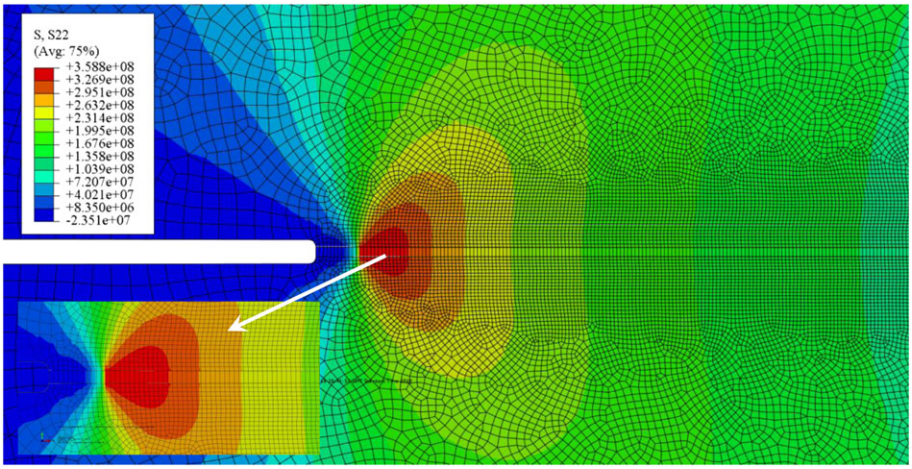

FIGURE 14 Stress field (measured in Pascal) with 140 cohesive elements used in the cohesive zone [Colour figure can be viewed at wileyonlinelibrary.com]

for one cycle and applied over ΔN cycles and then updated automatically for the next loading cycle. Another advantage of the model is that ΔN is automatically set according to the problem (low or high cycle fatigue) and incorporates a technique to evaluate the accurate number of cycles at failure rather than simply assuming it is a multiple of ΔN.

5 | CONCLUSIONS AND FUTURE WORKS

- A new trapezoidal CZM for fatigue that can be applied for high and low cycle fatigue simulations has been introduced.
- Decreasing the value of N^{u} is observed to lower crack growth. If, however, N^{u} is set so that the damage variable is sufficiently updated (after 800 cycles proved sufficient in the tests), then the results can be expected to be in good agreement with the experimental data with significant reduction in computational costs.
- The new CZM model has been shown to provide acceptable results with a significant reduction in the cost in terms of the computational time of the order of ΔN^{-1}.
- It is observed that the model tends to overestimate the crack length at crack initiation for crack lengths less than 1.2 mm, but subsequently, the predicted crack length is in line with experimental data.
- Additional experimental testing is needed to provide additional evidence on the uniqueness of the dimensionless material parameter C.
- The new procedure has only been tested under mode I loading conditions, but good outcomes are anticipated for mixed-mode analysis.

ACKNOWLEDGEMENTS

The authors would like to acknowledge the Higher Committee for Education Development in Iraq for funding Sarmed Salih and the College of Engineering at Babylon University for providing support for Sarmed Salih to facilitate his doctoral research at the University of Manchester.

ORCID

Sarmed Salih http://orcid.org/0000-0003-4278-0538

REFERENCES

1. Farahmand B. *Virtual Testing and Predictive Modeling*. Springer Science+Business Media; 2009 http://link.springer.com/content/pdf/10.1007/978-0-387-95924-5.pdf. Accessed March 3, 2014.
2. Li H, Yuan H. Cohesive zone modelling of low cycle fatigue cracks in cracked and notched specimens. *Fatigue Fract Eng Mater Struct*. 2013;36(12):1246-1257. https://doi.org/10.1111/ffe.12061
3. Robinson P, Galvanetto U, Tumino D, Bellucci G, Violeau D. Numerical simulation of fatigue-driven delamination using interface elements. *Int J Numer Methods Eng*. 2005;63(13):1824-1848. https://doi.org/10.1002/nme.1338
4. Tumino D, Cappello F. Simulation of fatigue delamination growth in composites with different mode mixtures. *J Thermoplast Compos Mater*. 2007;41(20):2415-2441. https://doi.org/10.1177/0021998307075439
5. Turon A, Costa J, Camanho P, Mayugo J. Simulation of delamination propagation in composites under high-cycle fatigue by means of cohesive zone models. NASA Tech Rep. 2006. http://www.iccm-central.org/Proceedings/ICCM16proceedings/contents/pdf/WedG/WeGA1-03sp-turona225067p.pdf.
6. Turon A, Costa J, Camanho PP, Dávila CG. Simulation of delamination in composites under high-cycle fatigue. *Compos Part A Appl Sci Manuf*. 2007;38(11):2270-2282. https://doi.org/10.1016/j.compositesa.2006.11.009
7. Pirondi A, Moroni F. A progressive damage model for the prediction of fatigue crack growth in bonded joints. *J Adhes Dent*. 2010;86(5–6):501-521. https://doi.org/10.1080/00218464.2010.484305
8. Harper PW, Hallett SR. A fatigue degradation law for cohesive interface elements—development and application to composite materials. *Int J Fatigue*. 2010;32(11):1774-1787. https://doi.org/10.1016/j.ijfatigue.2010.04.006
9. Pirondi A, Moroni F. Simulation of mixed-mode I/II fatigue crack propagation in adhesive joints with a modified cohesive zone model. *J Adhes Sci Technol*. 2011;25(18):2483-2499. https://doi.org/10.1163/016942411X580180
10. Bak BLV, Turon A, Lindgaard E, Lund EA. Benchmark study of simulation methods for high-cycle fatigue-driven delamination based on cohesive zone models. *Compos Struct*. 2016;164:198-206. https://doi.org/10.1016/j.compstruct.2016.11.081
11. Bak BLV, Sarrado C, Turon A, Costa J. Delamination under fatigue loads in composite laminates: a review on the observed phenomenology and computational methods. *Appl Mech Rev*. 2014;66(6). https://doi.org/10.1115/1.4027647, 060803
12. de Moura MFSF, Gonçalves JPM. Cohesive zone model for high-cycle fatigue of adhesively bonded joints under mode I loading. *Int J Solids Struct*. 2014;51(5):1123-1131. https://doi.org/10.1016/j.ijsolstr.2013.12.009
13. De Moura MFSF, Gonçalves JPM. Development of a cohesive zone model for fatigue/fracture characterization of composite bonded joints under mode II loading. *Int J Adhes Adhes*. 2014;54:224-230. https://doi.org/10.1016/j.ijadhadh.2014.07.002
14. Liu J, Li J, Wu B. The cohesive zone model for fatigue crack growth. *Adv inMechanical Eng*. 2013.
15. Kuna M, Roth S. General remarks on cyclic cohesive zone models. *Int J Fract*. 2016;196(1-2):147-167. https://doi.org/10.1007/s10704-015-0053-y

16. Zan DQ, Sun Q, Pan HL, Chen JJ, Wang ZD. Application of the cohesive zone model for analysing the edge crack propagation of steel sheet in the cold rolling process. *Fatigue Fract Eng Mater Struct*. 2017;40(6):869-881. https://doi.org/10.1111/ffe.12548
17. Khoramishad H, Crocombe AD, Katnam KB, Ashcroft IA. Predicting fatigue damage in adhesively bonded joints using a cohesive zone model. *Int J Fatigue*. 2010;32(7):1146-1158. https://doi.org/10.1016/j.ijfatigue.2009.12.013
18. De-Andrés A, Pérez J, Ortiz M. Elastoplastic finite element analysis of three-dimensional fatigue crack growth in aluminum shafts subjected to axial loading. *Int J Solids Struct*. 1999;36(15):2231-2258. http://www.sciencedirect.com/science/article/pii/S0020768398000596. Accessed April 8, 2014
19. Nguyen O, Repetto E. A cohesive model of fatigue crack growth. *Int J Fract*. 2001;110(4):351-369. http://link.springer.com/article/10.1023/A:1010839522926. Accessed March 21, 2014.
20. Yang B, Mall S, Ravi-Chandar K. A cohesive zone model for fatigue crack growth in quasibrittle materials. *Int J Solids Struct*. 2001;38(22–23):3927-3944. https://doi.org/10.1016/S0020-7683(00)00253-5
21. Roe KL, Siegmund T. An irreversible cohesive zone model for interface fatigue crack growth simulation. *Eng Fract Mech*. 2003;70(2):209-232. https://doi.org/10.1016/S0013-7944(02)00034-6
22. Beaurepaire P, Schuëller GI. Modeling of the variability of fatigue crack growth using cohesive zone elements. *Eng Fract Mech*. 2011;78(12):2399-2413. https://doi.org/10.1016/j.engfracmech.2011.05.011
23. Ural A, Krishnan VR, Papoulia KD. A cohesive zone model for fatigue crack growth allowing for crack retardation. *Int J Solids Struct*. 2009;46(11–12):2453-2462. https://doi.org/10.1016/j.ijsolstr.2009.01.031
24. Khoramishad H, Crocombe AD, Katnam KB, Ashcroft IA. Fatigue damage modelling of adhesively bonded joints under variable amplitude loading using a cohesive zone model. *Eng Fract Mech*. 2011;78(18):3212-3225. https://doi.org/10.1016/j.engfracmech.2011.09.008
25. Towashiraporn P, Subbarayan G, Desai CS. A hybrid model for computationally efficient fatigue fracture simulations at microelectronic assembly interfaces. *Int J Solids Struct*. 2005;42(15):4468-4483. https://doi.org/10.1016/j.ijsolstr.2004.12.012
26. Koutsourelakis PS, Kuntiyawichai K, Schuëller GI. Effect of material uncertainties on fatigue life calculations of aircraft fuselages: a cohesive element model. *Eng Fract Mech*. 2006;73(9):1202-1219. https://doi.org/10.1016/j.engfracmech.2006.01.003
27. Tvergaard V, Hutchinson JW. The relation between crack growth resistance and fracture process parameters in elastic-plastic solids. *J Mech Phys Solids*. 1992;40(6):1377-1397. https://doi.org/10.1016/0022-5096(92)90020-3
28. Salih S, Davey K, Zou Z. Rate-dependent elastic and elasto-plastic cohesive zone models for dynamic crack propagation. *Int J Solids Struct*. 2016;90:95-115. https://doi.org/10.1016/j.ijsolstr.2016.04.002
29. Schwalbe K, Scheider I, Cornec A. *Guidelines for Applying Cohesive Models to the Damage Behaviour of Engineering Materials and Structures*. Berlin, Heidelberg: Springer Berlin Heidelberg; 2013. doi:https://doi.org/10.1007/978-3-642-29494-5
30. Falk ML, Needleman A, Rice JR. A critical evaluation of cohesive zone model of dynamic fracture. In: Proceedings of the 5th, Journal de Physique IV, Proceedings 11(Pr.5). ; 2001:43–50. http://arxiv.org/abs/cond-mat/0106304.
31. Zhang X, Mai Y-W, Jeffrey RG. A cohesive plastic and damage zone model for dynamic crack growth in rate-dependent materials. *Int J Solids Struct*. 2003;40(21):5819-5837. https://doi.org/10.1016/S0020-7683(03)00370-6
32. Alfano G, De Barros S, Champaney L, Valoroso N. Comparison between two cohesive-zone models for the analysis of interface debonding. *Eur Congr Comput Methods Appl Sci Eng*. 2004;1-18. http://imechanica.org/files/Alfano-Barros-Champaney-Valoroso-ECCM04.pdf
33. Scheider I, Schödel M, Brocks W, Schönfeld W. Crack propagation analyses with CTOA and cohesive model: comparison and experimental validation. *Eng Fract Mech*. 2006;73(2):252-263. https://doi.org/10.1016/j.engfracmech.2005.04.005
34. ABAQUS. *ABAQUS 6.13 User Guide*. USA: Dassault Systèmes Simulia Corp; 2013 http://129.97.46.200:2080/v6.13/.
35. Bak BL V, Lindgaard E, Lund E, Turon A. Performance of cohesive zone models for fatigue driven delaminations. In: *11th World Congress on Computational Mechanics*; 2014:1–2.

How to cite this article: Salih S, Davey K, Zou Z. A computationally efficient cohesive zone model for fatigue. *Fatigue Fract Eng Mater Struct*. 2018;1–15. https://doi.org/10.1111/ffe.12927